Inhomogeneous precipitation distribution and snow transport in steep terrain

M. Lehning,[1] H. Löwe,[1] M. Ryser,[1] and N. Raderschall[1]

Received 22 September 2007; revised 12 January 2008; accepted 1 February 2008; published 3 July 2008.

[1] The inhomogeneous snow distribution found in alpine terrain is the result of wind and precipitation interacting with the (snow) surface over topography. We introduce and explain preferential deposition of precipitation as the deposition process without erosion of previously deposited snow and thus in absence of saltation. A numerical model is developed, describing the relevant processes of saltation, suspension, and preferential deposition. The model uses high-resolution wind fields calculated with a meteorological model, ARPS. The model is used to simulate a 120 h snow storm period over a steep alpine ridge, for which snow distribution measurements are available. The comparison to measurements shows that the model captures the larger-scale snow distribution patterns and predicts the total additional lee slope loading well. However, the spatial resolution of 25 m is still insufficient to capture the smaller-scale deposition features observed. The model suggests that the snow distribution on the ridge scale is primarily caused by preferential deposition and that this result is not sensitive to model parameters such as turbulent diffusivity, drift threshold, or concentration in the saltation layer.

Citation: Lehning, M., H. Löwe, M. Ryser, and N. Raderschall (2008), Inhomogeneous precipitation distribution and snow transport in steep terrain, *Water Resour. Res.*, *44*, W07404, doi:10.1029/2007WR006545.

1. Introduction

[2] Snow transport by wind is one of the crucial factors influencing the seasonal buildup of the snow cover in alpine terrain and the related avalanche activity. In addition to avalanche danger, local hydrology, mass balance of glaciers and vegetation development are also heavily influenced by spatially varying snow distribution. Because of its importance, snow transport has been studied intensively over the last few decades. Despite these efforts, operational assessments of snow redistribution by the wind hardly exist because of the complexity of the physical processes associated with this phenomenon. Drifting snow representation in current models is therefore often rudimentary and neglects processes which are known to have a significant influence, especially in complex terrain. In this introduction, we discuss the current understanding of the processes saltation, suspension and snow cover.

[3] For snow drift, we usually distinguish between grains being transported in reptation or creep, saltation or suspension mode. Reptation is the rolling of particles over the surface and the associated mass flux is usually small compared to the latter two processes. We therefore do not discuss creep here. Saltation takes place in a thin layer directly above the surface, where the particle concentration is highest. In this transport mode the snow grains follow ballistic trajectories and return to the surface, possibly rebounding or ejecting other grains. For the mass flux in saltation, many investigators [*Bagnold*, 1941; *Takeuchi*, 1980; *Pomeroy and Gray*, 1990] have made efforts to find empirical relations based on measurements and physical considerations. Only more recently, numerical models have been developed [*McEwan and Willets*, 1991; *Shao and Li*, 1999; *Nemoto and Nishimura*, 2004] which take into account the microscopic processes of aerodynamic entrainment, particle-bed collisions, particle motion and particle-wind feedback. A model that explicitly takes into account the effect of the slope on saltation has been developed by *Doorschot and Lehning* [2002] and *Doorschot et al.* [2004].

[4] For obtaining the mass transport in suspension, a mass conservation equation for the snow particles needs to be solved in combination with the Navier Stokes equations for the turbulent air flow. A promising alternative approach is the use of a Lagrangian dispersion formulation to represent snow in suspension [*Sato et al.*, 1997; *Sundsbø and Hansen*, 1997]. However, to the author's knowledge, such promising first attempts have not further been pursued recently. In current models, suspension is often simplified by assuming it to be in equilibrium with the underlying saltation and ignoring lateral advective effects, so that a one-dimensional diffusion equation remains [*Kind*, 1992; *Liston and Sturm*, 1998]. The most integrative model on snow transport has been presented by *Gauer* [2001], who applied a model of flow simulation, saltation and suspension to a high alpine ridge. His model based on the CFX flow solver already contained most of the important processes except for the snow cover development. The high integration and coupling between flow and transport simulation rendered verification of the individual model modules difficult, however. Therefore, it was difficult to explain differences between the model simulations and measurements of snow distribution.

[1]WSL, Swiss Federal Institute for Snow and Avalanche Research, SLF Davos, Davos, Switzerland.

0043-1397/08/2007WR006545

[5] Enhanced sublimation during drifting snow has been discussed extensively for arctic regions [*Bintanja*, 2001; *Déry and Yau*, 2002]. While the overall quantitative effect on the moisture budget is still in debate, we exclude this effect in the analysis presented here. We focus on precipitation events, during which additional sublimation due to drifting snow can be neglected.

[6] However, we want to focus on an effect, which to our knowledge has not been analyzed and discussed in detail thus far. We call this effect preferential deposition. While already [e.g., *Meister*, 1987, p. 273] notes that "drift flux is a mixing of precipitation and rounded surface snow particles, which by creeping, saltation or diffusion are ejected into the air flow," the inhomogeneous precipitation deposition in the absence of local erosion has never been investigated separately. We define preferential deposition therefore as the spatially varying deposition of (liquid and solid) precipitation due to the topography induced flow field modification close to the surface. We investigate the contribution of preferential deposition to the loading of avalanche slopes during snow fall events. Little is known about this tendency of precipitation to accumulate directly in leeward slopes, and this process has never been investigated on its own, although in principle it is included in every three-dimensional suspension model.

[7] Finally, for the simulation of drifting snow the development of the snow cover needs to be considered at sites of erosion and deposition. The snow type has a strong influence on the drift, since it affects model parameters like threshold shear velocity, effectiveness of rebound during saltation and the particle size distribution. In a windward slope, freshly fallen snow may be eroded until the old layer of snow with a higher threshold has been reached, thus providing an upper limit for the total mass transport. On the other hand, new snow that has been transported by the wind is mechanically altered. While a detailed treatment of snow properties has been introduced to simple drift index calculations [*Lehning and Fierz*, 2007], three-dimensional snow drift models [*Liston et al.*, 2007] have typically a very simple snow representation.

[8] In this paper we present a new numerical model (Alpine3D) for the estimation of snow distribution in steep alpine terrain due to blowing and drifting snow and compare it to own field measurements. We discuss the processes involved and present corresponding model descriptions or reference known work. The wind field simulations are treated in a companion paper. Since preferential deposition is discussed for the first time at length, we use an analytical model of preferential deposition to demonstrate some aspects of this process. We compare model simulations of snow distribution with observed snow distribution at small scale and at the hillslope scale. Finally, we present the model results for the relative contributions of the individual transport processes in order to discuss the importance of preferential deposition.

2. Processes and Model Description

2.1. Calculation of Wind Fields

[9] The influence of topography on the wind field and the local energy balance are the main factors for a spatially varying snow distribution. For our goal of describing snow variability in very steep terrain, simple local adaptation schemes for the local wind speed [*Liston and Sturm*, 1998] appear not to be adequate because they cannot describe critical flow features of steep terrain such as blocking or flow separation. To obtain the high-resolution wind field over complex topography we use the mesoscale atmospheric model Advanced Regional Prediction System (ARPS) [*Xue et al.*, 1995] in its SUBMESO version. The topography in the presented case is a mountain ridge with slope angles between 30 and 50 degrees, which is typical for avalanche slopes. In the 25 m resolution of the digital elevation model used here, maximum slope angles of 45 degrees are present. In ARPS, the nonhydrostatic compressible Navier-Stokes equations for turbulent air flows are solved on a mesh, using the finite differences method. Novel is the use of a mesoscale atmospheric model with a resolution down to 25 m for strong wind conditions. The flow field simulations are discussed in detail in a companion paper [*Raderschall et al.*, 2008]. We only use the mean flow characteristics of the wind field for the application described here and parameterize turbulence in our drift model from similarity theory. As discussed by *Raderschall et al.* [2008], we consider the flow field to represent the mean flow features after a short flow integration of 30 s. For longer integration times, turbulent structures develop and an averaging operation over a long time period would be required to recover the mean flow. For practical reasons, we have therefore chosen to regard the initial adaptation of the flow to the topography as a good approximation of the mean flow.

[10] Particular is the wind classification that we deploy to limit the calculation effort for the wind field simulations. Not a full time evolution of the atmospheric flow field is calculated but the simulation time is decomposed into pieces of quasi-stationary conditions. For chosen time intervals (at present 1 h), we model a stationary wind field with ARPS using the time-averaged measurements to prescribe initial and boundary conditions. Figure 1 shows the time series of wind speed and direction upwind of the ridge. This measured evolution has been manually and arbitrarily decomposed into the nominal wind fields given in Table 1. These nominal wind fields have a directional resolution of 45° and are calculated for three nominal speeds (1: light; 3: medium; 6: strong; 9: very strong). The missing meteorological parameters such as precipitation rates and temperature are taken from measurements. From ARPS, the three-dimensional wind velocity field is then known at each grid point.

2.2. Saltation Layer

[11] For calculating the snow mass that is transported in the saltation layer, we use the physical model of *Doorschot and Lehning* [2002], which has thus far only been applied to a point analysis of drifting snow [*Doorschot et al.*, 2004] and to wind tunnel data [*Clifton et al.*, 2007].

[12] One of its new features is the consideration of the influence of a sloping bottom. Furthermore, the effects of particle-wind feedback, particle trajectories and grain properties are included. Here we only summarize the main model features. A full description is available from *Doorschot and Lehning* [2002] and *Clifton and Lehning* [2008]. Saltation is

regarded as a self-regulating process which develops to equilibrium because of the modification of the wind field by the transfer of particle momentum. Saltation starts when the shear stress at the surface exceeds the threshold shear stress for aerodynamic entrainment. The number of saltating particles then increases rapidly, until the maximum capacity that the air flow can carry is reached. Numerical simulations suggest that this steady state is reached within a time of 1–2 s [*Nemoto and Nishimura*, 2004]. In principle there are three different ways for a snow particle to start a trajectory in saltation: aerodynamic entrainment, rebound from a previous impact, or ejection by the impact of an other grain. In a saltation layer at equilibrium, there exists a statistical balance between a small probability of a grain not rebounding after impact and the also small probability of a new grain being dislodged with enough energy to start saltating such that the mean replacement capacity is one. Within the saltation layer, the flying grains exert a stress on the air flow, the so-called grain borne shear stress, which is defined as the difference in horizontal momentum between upgoing and downgoing particles at a certain height. At steady state, the sum of the grain borne and fluid (or air borne) shear stresses equals the total shear stress above the saltation layer [*McEwan and Willets*, 1991]. At equilibrium, the mean replacement capacity is one, and this can only be the case if the air borne shear stress at the surface stays at impact threshold [*Owen*, 1964]. Furthermore, above the saltation layer, the air borne shear stress has to approach the total boundary layer shear stress.

[13] Calculating grain trajectories for a range of shear stresses [*Doorschot et al.*, 2004] and parameterizing feedback on the flow [*McEwan*, 1993], a stationary mass flux formulation can be obtained by iteration as reviewed by *Clifton and Lehning* [2008]. Additionally, a reference saltation concentration is obtained, which serves as a lower boundary condition for suspension in the presence of saltation. The reference concentration is calculated by considering the mass of snow particles in the air at the saltation height:

$$h_s = z_0 + \frac{(u_e \cos(\alpha_e))^2}{4g}. \tag{1}$$

[14] Here, z_0 is the roughness length, $u_e = 3.1u*$ and $\alpha_e = 25°$ are ejection velocity and angle, respectively, which have been found by matching the observed to modelled mass flux [*Doorschot et al.*, 2004]; g is the acceleration of gravity. Then, from a momentum balance, the difference between a regular log wind profile and the wind profile ($\Delta U(z)$) in the presence of drifting particles determines the concentration:

$$c_{\mathrm{salt}}(z = h_s) = \frac{\rho_{air}(\Delta U(z))^2}{u^2_{mean}}, \tag{2}$$

where u^2_{mean} is the mean velocity of the drifting particles. Depending on the flow and snow conditions, the mass flux calculation may require many iterations [*Clifton and Lehning*, 2008], which has not been observed for the wind fields discussed here.

[15] An important parameter of any saltation model is the threshold friction velocity. Since Alpine3D calculates the complete development of the snow cover at every grid point, the friction velocity can very with the surface snow characteristics. This feature has been shown to be important for the calculation of a drift index for avalanche warning [*Lehning and Fierz*, 2007] and is the most important contribution of the snow module (in addition to snow settling) for the application of Alpine3D discussed here. Note that saltation is computed independently at each grid point.

2.3. Suspension Layer and Preferential Deposition

[16] Snow particles in the suspension layer stem from snow fall (influx through top and lateral boundaries) and the saltation layer (influx through the bottom boundary layer). Although their respective forms can vary a lot, we assume them to be equally shaped and neglect possible differences in morphology. The suspended snow crystals are modeled as passive, heavy tracers. The feedback of suspended crystals on wind flow as well as intercrystal interactions are neglected. During the simulation, the wind field is updated every hour and assumed to be stationary between the updates. In order to be consistent with this quasi-stationary wind field, the transport of suspended snow is assumed to be stationary during the chosen intervals and is updated on an hourly basis together with the wind field. Thus, the concentration $c(\mathbf{x})$ of snow mass is governed by the stationary advection-diffusion equation

$$\nabla \cdot (K(\mathbf{x})\nabla c(\mathbf{x})) - \mathbf{u}_{\mathrm{p}}(\mathbf{x}) \cdot \nabla c(\mathbf{x}) = 0. \tag{3}$$

Here, ∇ denotes the gradient, $\mathbf{u}_{\mathrm{p}}$ is the particle velocity field with vanishing divergence and $K(\mathbf{x})$ the (diagonal) matrix of turbulent diffusivity. The velocity field $\mathbf{u}_{\mathrm{p}} = (u, v, w - w_s)$ comprises the stationary solution of the wind simulation (u, v, w) from ARPS and the mean settling velocity w_s which is assumed to be independent of position. The settling velocity can in principle be calculated from the force balance on an individual particle with an appropriate drag law. For the application discussed here, we work with an uniform grain size and a fixed mean settling velocity of 0.5 m s^{-1}. The diagonal elements K_i for $i = x, y, z$ of the turbulent diffusion matrix are parameterized by the following model diffusivity [*Xiao et al.*, 2000]

$$K_i(\mathbf{x}) = |\nabla u(\mathbf{x})| \left(\frac{1}{k(z + z_0)} + \frac{1}{l_i} \right)^{-2} \tag{4}$$

with the length scale l_i determined by the grid spacing and the von Karman constant, $k = 0.4$. Since this expression may give too small values close to the ground because of its dependence on the vertical coordinate, z, a lower limit to K_i, the neutral surface layer similarity expression is introduced:

$$K_{\mathrm{lim}}(\mathbf{x}) = kzu*. \tag{5}$$

[17] To avoid problems with zero wind velocities at some grid points (stagnation points), a lower limit of the friction velocity of 0.1 m s^{-1} is assumed.

[18] To define the model completely, it remains to specify the boundary conditions which determine the overall mass balance in the simulation domain. In principle, precipitation

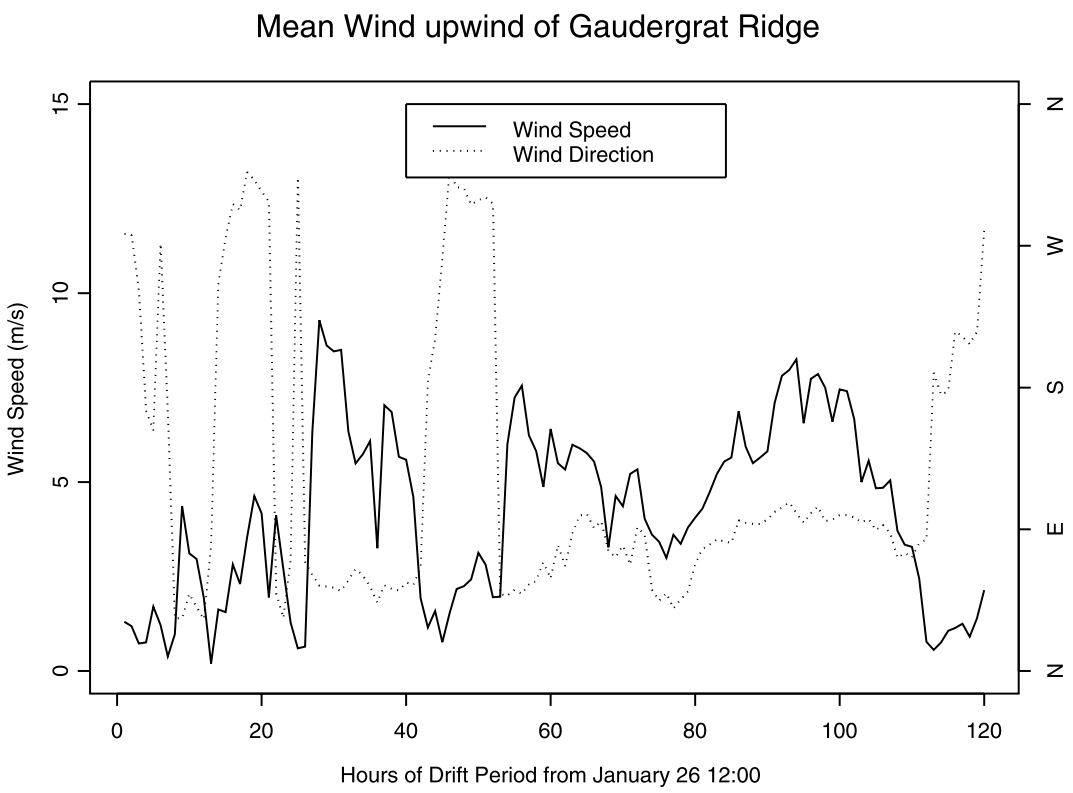

Figure 1. Time series of wind upwind of the ridge during 5 d of the snowstorm period in January 1999.

and erosion by saltation constitute the available mass which is then redistributed by equation (3).

[19] We assume that the computational domain is large enough to not disturb the precipitation field at the boundaries. On the basis of this assumption, we imply homogeneous Dirichlet conditions on the upper and lateral boundaries of the domain and the corresponding value of the concentration is determined by the homogeneous precipitation flux q_0, i.e., $c(\mathbf{x}) = c_{\text{prec}} := q_0/w_s$.

[20] On the lower boundary the snow concentration is determined by specifying the normal flux $q^{\perp}_{\text{susp}}(\mathbf{x}) := \mathbf{n}(\mathbf{x}) \cdot (-K(\mathbf{x})\nabla c(\mathbf{x}) + \mathbf{u}_p(\mathbf{x})c(\mathbf{x}))$ on the boundary. The normal vector field $\mathbf{n}(\mathbf{x})$ on the lower boundary is directed outward such that a positive contribution to q represents an outward mass flux, i.e., a deposition. The normal flux is decomposed into two contributions

$$q^{\perp}_{\text{susp}}(\mathbf{x}) = q^{\perp}_{s}(\mathbf{x}) + q^{\perp}_{\text{exc}}(\mathbf{x}). \tag{6}$$

The first contribution, $q^{\perp}_{s}(\mathbf{x})$, represents the gravitational fall of particles across the boundary, i.e., $q^{\perp}_{s}(\mathbf{x}) = w^{\perp}_{s}\, c(\mathbf{x})$ where $w^{\perp}_{s}$ is the normal component of the settling velocity. The second contribution stems from mass exchange with the saltation layer. We assume that it is driven by the difference in concentration, i.e., $q^{\perp}_{\text{exc}}(\mathbf{x}) = K^{\perp}(\mathbf{x})/h_{\text{ref}}[c(\mathbf{x}) - (c_{\text{salt}}(\mathbf{x}) + c_{\text{prec}})]$. Whenever the concentration $c(\mathbf{x})$ deviates from the concentration c_{salt} in the saltation layer modified by the background precipitation concentration a resulting mass flux occurs which is driven by the component $K^{\perp}$ of diffusion normal to the surface. For simplicity, the reference height is taken to be $h_{\text{ref}} = 1$ m throughout our simulations. Using the fact that the ARPS wind field (u, v, w) has vanishing normal component at the boundary we are led to a boundary condition of Robin type

$$-\mathbf{n}(\mathbf{x}) \cdot K(\mathbf{x})\nabla c(\mathrm{x}) = \frac{K^{\perp}(\mathbf{x})}{h_{\text{ref}}}\left[c(\mathbf{x}) - \left(c_{\text{salt}}(\mathbf{x}) + c_{\text{prec}}\right)\right] \tag{7}$$

for all points $\mathbf{x}$ on the bottom boundary.

[21] The mass conservation equation (3) is solved numerically by a finite element method. Since the equation is highly advection dominated, we used a streamline upwind/Petrov-Galerkin scheme for stabilization [*Brooks and Hughes*, 1982]. The finite elements are given by the hexahedral ARPS mesh and we use linear shape functions. The resulting linear system is solved with a biconjugate gradient method with (diagonal) preconditioner.

2.4. Snow Cover Characteristics: SNOWPACK

[22] SNOWPACK is a finite element–based physical snow cover model, which is in operational use in connection with the Swiss network of approximately 150 high alpine automatic snow and weather stations [*Lehning et al.*, 1999]. It solves the heat transfer and snow settlement equations and calculates phase changes and transport of water vapor and liquid water. Furthermore, it includes surface hoar formation and snow metamorphism (grain types). A complete description of the model can be found in work by *Bartelt and Lehning* [2002] and *Lehning et al.* [2002a, 2002b]. For the application described here, SNOWPACK has been coupled to our snow drift model for the assessment of the erodibility of the snow cover and the development of the snow cover at different locations due to erosion and deposition of snow. For determining the erodibility of the snow cover we follow

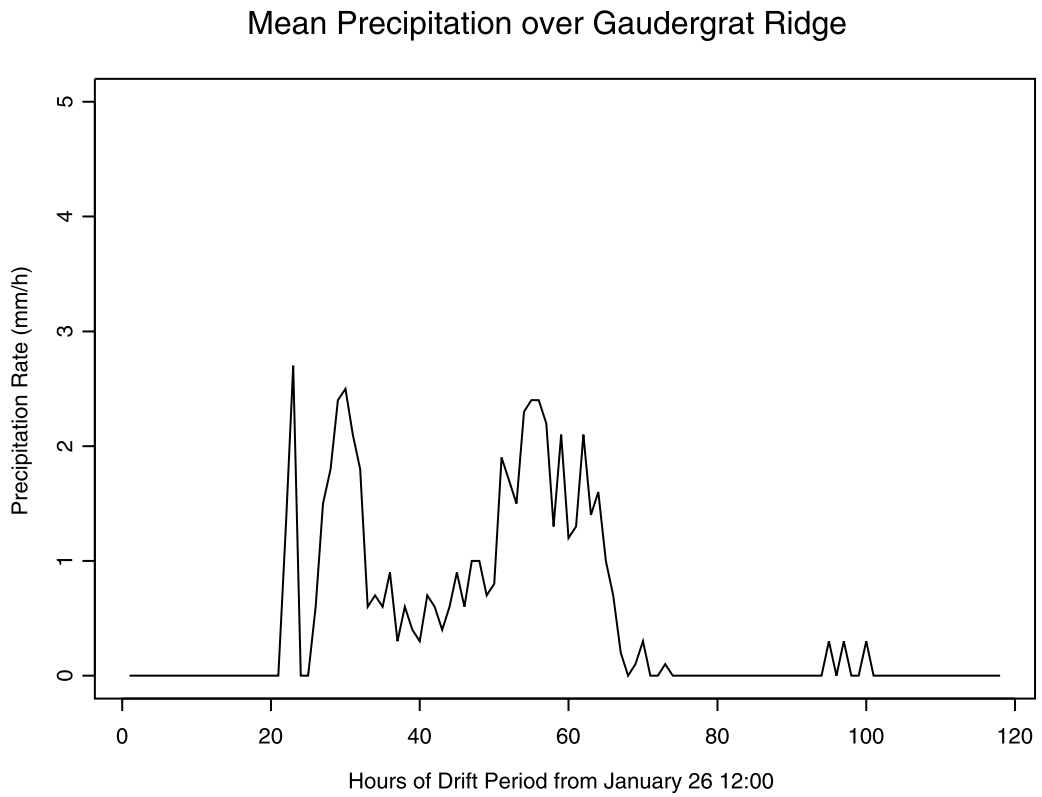

Figure 2. Mean precipitation during the snowstorm period in January 1999, derived from an independent run of SNOWPACK on the Kreuzweg IMIS station [*Lehning et al.*, 1999].

[*Schmidt*, 1980] and use the procedure as detailed by *Lehning and Fierz* [2007] to calculate the threshold friction velocity.

2.5. Erosion and Deposition

[23] The lower boundary of the computational domain for suspension and preferential deposition is of particular importance. In order to determine whether snow drift is possible or not, the shear velocity at the surface u^* has to be found. To this end, we simply use the logarithmic law of the wall neglecting stability and calculate the friction velocity from the velocity of the first grid point above the ground. Erosion at a grid cell will then only take place if $u^* > u^*_{\mathrm{th}}$ where the threshold value u^*_{th} is imposed by the snow cover.

[24] The overall deposition flux includes contributions from saltation and from suspension. For saltation we compute the erosion/deposition rate in units of kg m^{-2} s^{-1} by

$$q^{\perp}_{\mathrm{salt}}(x,y) = \frac{\partial}{\partial x} q_{\mathrm{salt}}(x,y) + \frac{\partial}{\partial y} q_{\mathrm{salt}}(x,y) \tag{8}$$

from the stationary mass flux q_{salt} given by the saltation model [*Clifton and Lehning*, 2008]. Note that q_{salt} is a line flux given in units of kg m^{-1} s^{-1}.

[25] The suspension contribution to deposition/erosion is given by $q^{\perp}_{\mathrm{susp}}$ in equation (6) and thus the total erosion/deposition rate is computed from

$$q^{\perp}_{\mathrm{dep}} = q^{\perp}_{\mathrm{salt}} + q^{\perp}_{\mathrm{susp}}, \tag{9}$$

subjected to the condition that erosion can take place if saltation is present at all, i.e., only if $u^* > u^*_{\mathrm{th}}$.

[26] Note, that our erosion/deposition model lacks the feedback of the suspension on the saltation concentration: At the lower boundary mass is exchanged between the

Table 1. Decomposition of Time Evolution Into Stationary Wind Fields

Hours of Drift Period	Nominal Wind Field[a]
1–8	W 1
9–12	NW 3
13–15	W 1
16–20	SW 3
21–23	NW 3
24–26	W 1
27–31	NW 9
32–41	NW 6
42–46	W 1
47–52	SW 3
53	NW 3
54–60	NW 6
61–73	N 6
73–79	NW 3
80–81	N 3
82–89	N 6
90–101	N 9
102–106	N 6
107–111	N 3
111–120	W 1

[a]Shown are direction and speed.

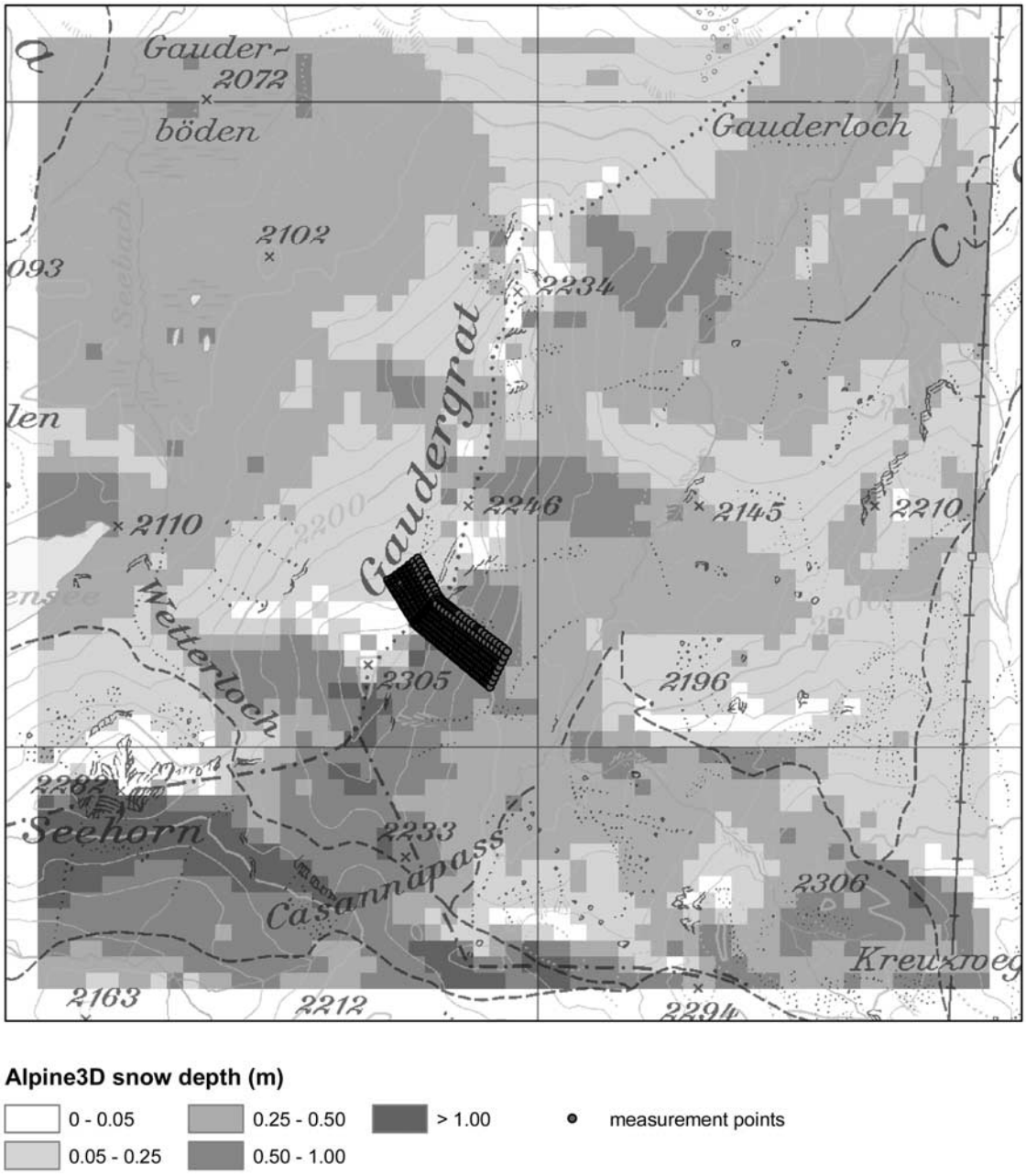

Figure 3. Simulated snow distribution (difference in snow depth after storm) at the end of the 120 h drift period of January 1999 for the full model domain. Simulation is for the reference run described in the text.

suspension phase and the saltation layer as implied by the BC in equation (7). Mass conservation would require to include this term as a source/sink for the saltation concentration (equation (2)). However, by calculating an equilibrium mass flux with the Doorschot saltation model this coupling is neglected.

[27] The drift module as described here is part of the Alpine3D model system for alpine surface processes. Alpine3D has previously been used for snow hydrology [*Lehning et al.*, 2006], without the drifting snow module. The grid for solving the diffusion equation (3) is currently chosen identical to the ARPS grid [*Raderschall et al.*, 2008]. Because of the terrain following coordinates in ARPS, the first grid level at the ridge is much closer to the surface than a grid level away from the ridge. In section 2.5, we describe how the erosion and deposition calculation needs a value of the wind vector "just above the saltation height." The saltation height varies significantly in space and time and therefore, we choose to use the wind vector at a fixed distance between the surface and the first grid level for this purpose. A model parameter between 0 and 1 determines the height of this level relative to the height of the first grid level. The parameter has the default value of 0.02 and is varied in the sensitivity studies described below.

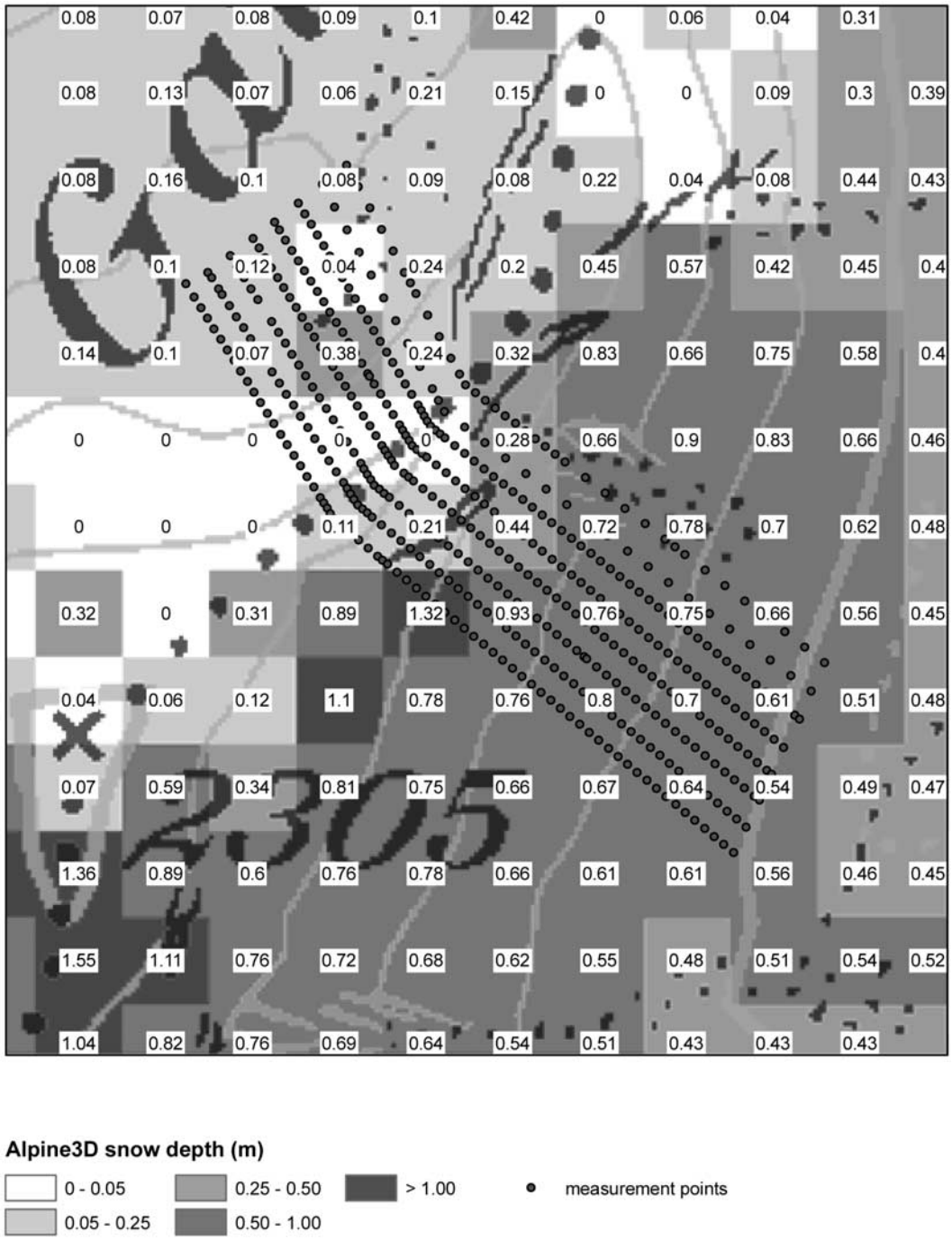

Figure 4. Simulated additional snow distribution from reference run at the end of the 120 h drift period at the end of January 1999 for the Gaudergrat subdomain. Simulation is for the reference run described in the text.

With this value, the lowest layer of the finite element grid varies approximately between 0.06 m at the crest and 0.3 m in terrain depressions, a range which is comparable to typical saltation heights.

3. Conceptual Description of Preferential Deposition

[28] Because preferential deposition of precipitation has obtained little attention in the past, we want to illustrate one part of this physical principle using simple considerations. A first observation is that snow deposition velocities vary with the terrain and the turbulence level and therefore also with the mean wind speed. The terrain causes local convergent and divergent flows, creates vorticity and local mean vertical velocities. Turbulence plays a role because vigorous turbulence causes significant relative velocities between the precipitation particles and the flow. Because of the nonlinearity of the particle-flow interaction any mean velocity of the particles is reduced by this effect. In an equilibrium

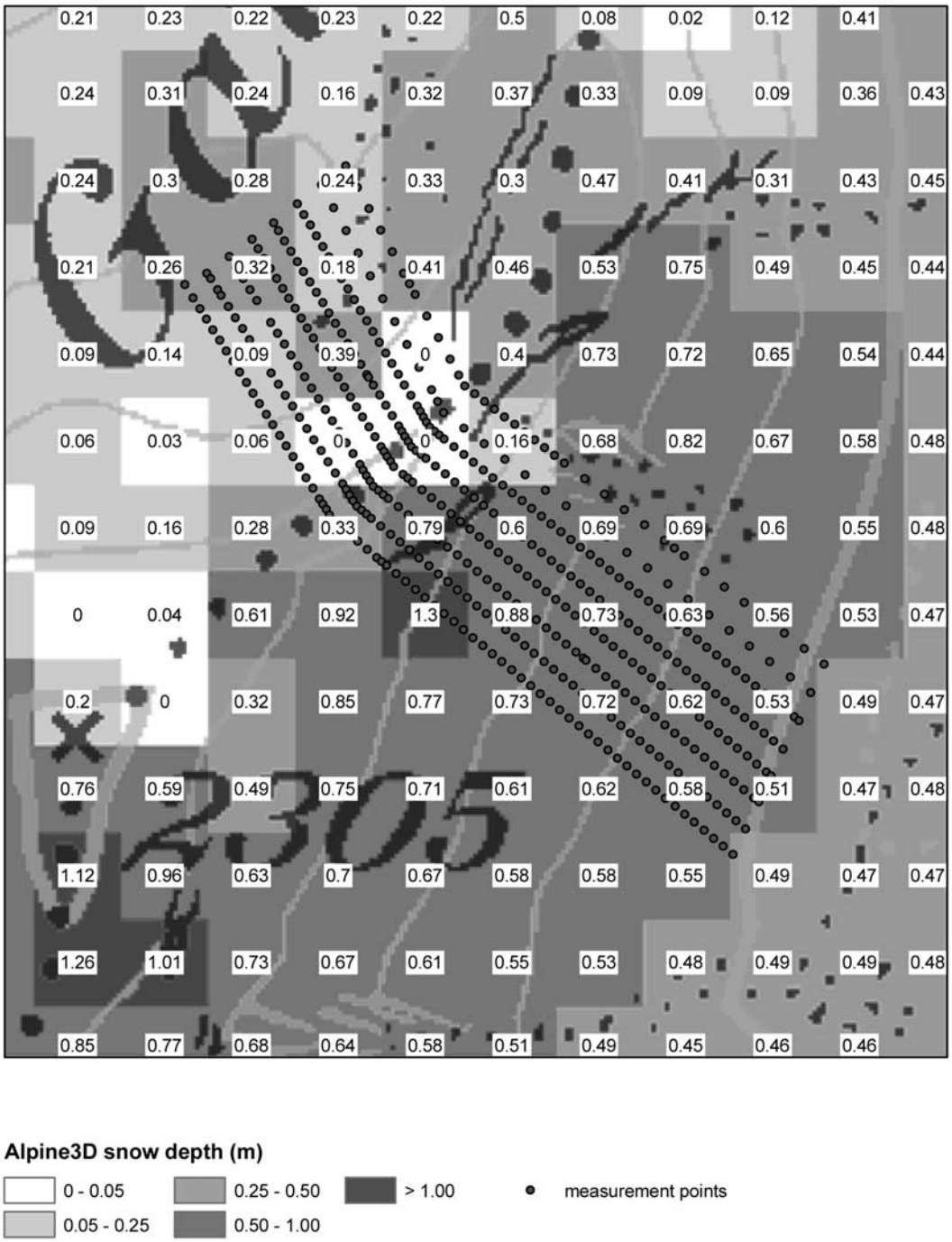

Figure 5. Simulated snow distribution for the Gaudergrat subdomain and a higher assumed settling velocity of 1.0 m s^{-1}.

treatment and based on similarity theory, this behavior can be formally expressed by introducing a velocity component reducing the settling velocity assuming isotropic turbulence:

$$w_s = w_{s0} - u^* \sqrt{\frac{10}{3}}, \tag{10}$$

where w_{s0} is the corresponding settling velocity in still air resulting from a force balance between weight and drag.

[29] This leads to the fact that the higher wind speeds and updrafts in the luff of a mountain ridge cause reduced deposition velocities there. However, note that equation (10) contains too much simplification of the real process, since in principle application of this equation could revert the settling velocity, which would be physically wrong. We therefore only postulate here that the settling velocity is reduced in the luff and increased in the lee and will use equation (10) below to get an order of magnitude estimate of the effect. A decreased deposition velocity on

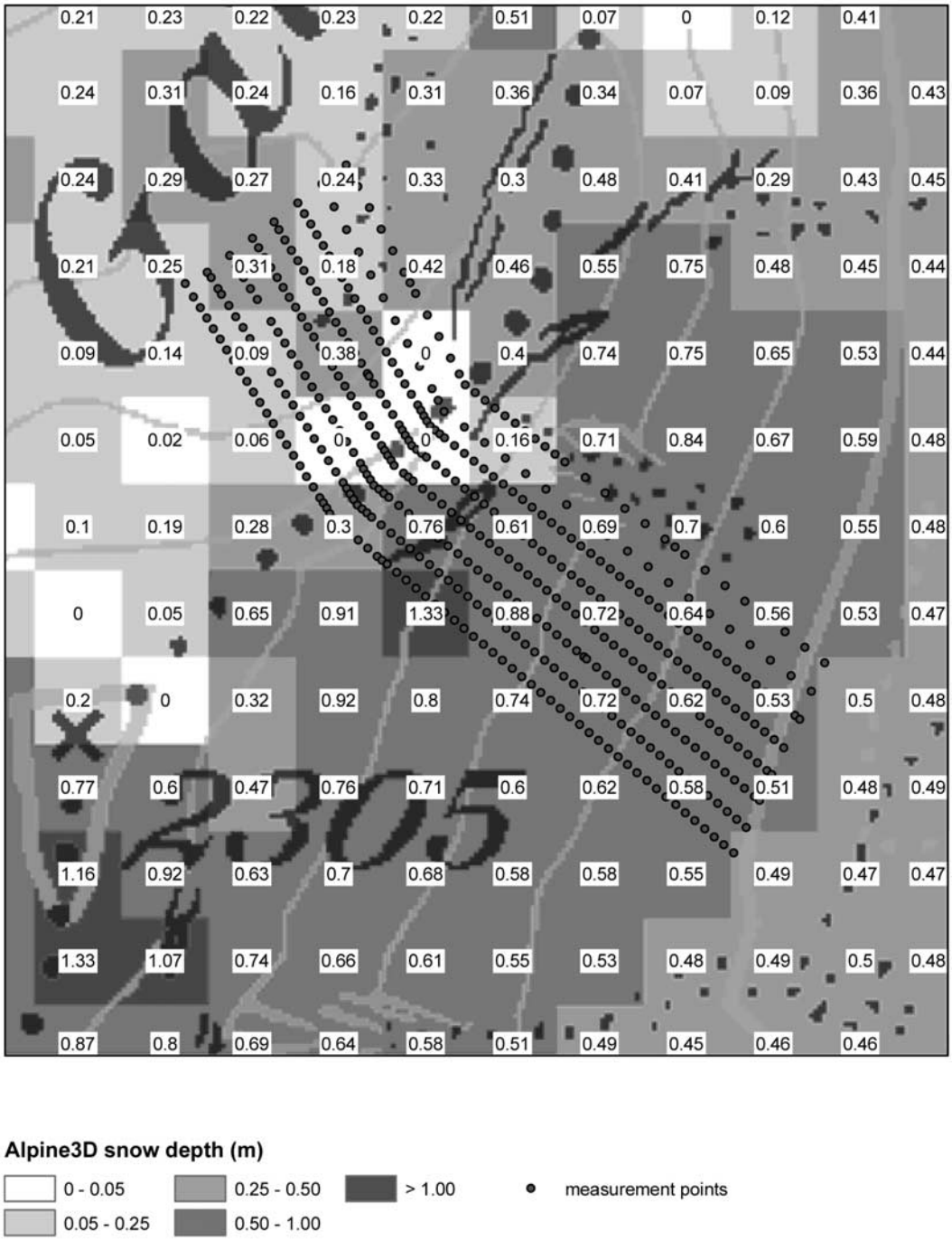

Figure 6. Simulated snow distribution for the Gaudergrat subdomain and a lower (50%) assumed threshold friction velocity for the onset of saltation.

the luff leads in turn to an accumulation of snow in an air parcel that travels uphill toward the crest. When the parcel then crosses the ridge, it enters an area of decreased wind velocity with higher deposition velocity and additionally has the accumulated higher concentration. These are two effects that cause uneven snow distribution in complex terrain during snow fall in the absence of local erosion. The effect of the deposition velocity translates linearly into an increased deposition in the lee slope. The effect of accumulation in a air parcel can also be better understood by the following considerations. We consider a parcel of air that travels uphill in the luff of a ridge. The parcel collects precipitation at the top boundary with the settling velocity, w_{s0} and the concentration of precipitation, c_0. Then the change in concentration in the parcel is described by

$$\frac{dc}{dt} = \frac{1}{h}(c_0 w_{s0} - c w_s). \tag{11}$$

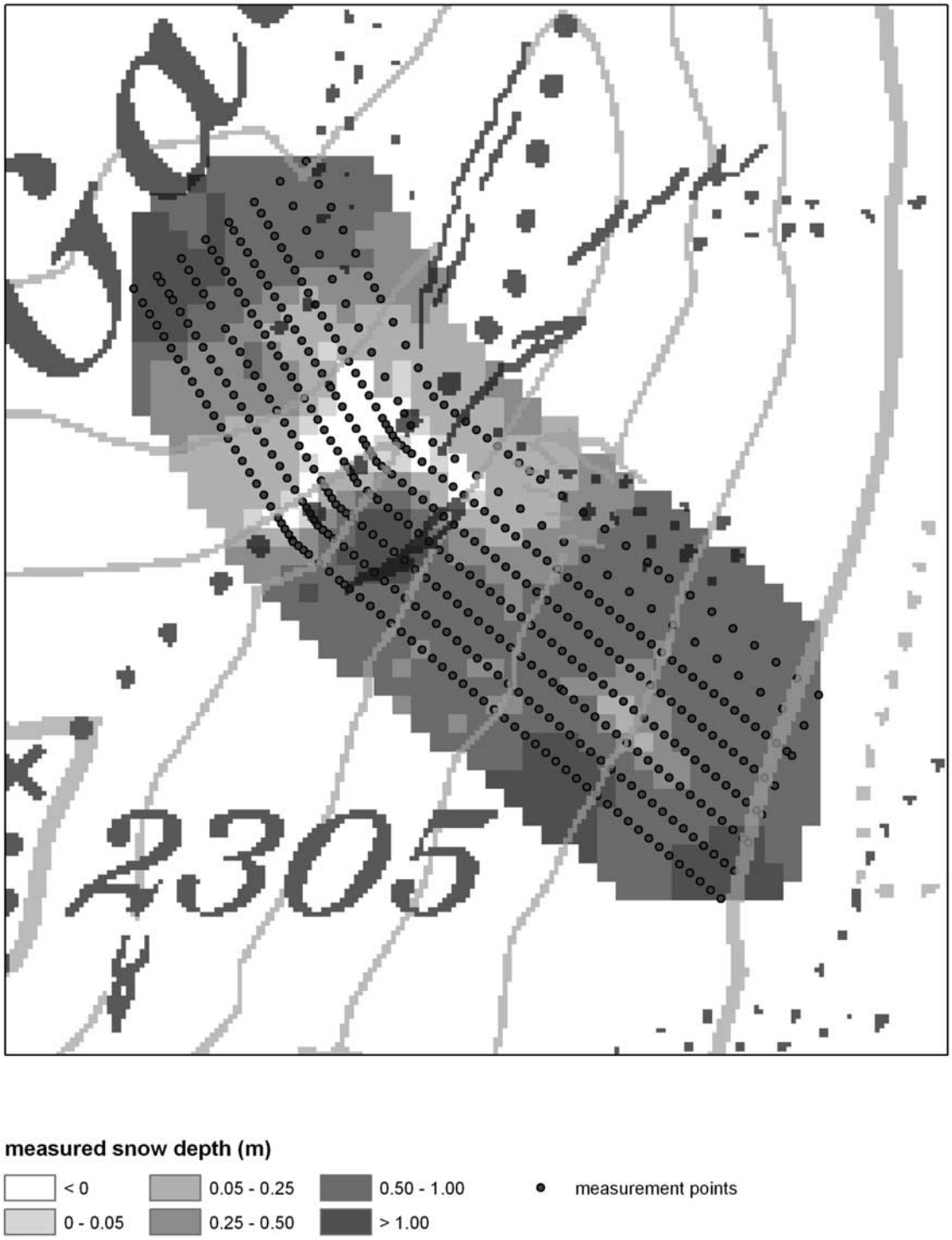

Figure 7. Measured snow distribution for a small stripe over the Gaudergrat ridge. Measurement points are shown by small dots. The ridge is indicated by large dots.

[30] Here h is the vertical depth of the parcel. For initial condition $c(0) = c_0$ the solution of equation (11) is given by

$$c(t)w_s = c_0 w_s + (w_{s0} - w_s)c_0\left(1 - e^{-\frac{w_s}{h}t}\right). \quad (12)$$

[31] It is important to note from equation (12) that the terrain only introduces a local disturbance in deposition. After some finite time (or distance), a new equilibrium between local settling velocity and concentration will be established, which leads to the same total deposition as prescribed by the local precipitation at some height.

[32] Investigating the magnitude of the two effects discussed above, we use some realistic numbers. We first note that typical settling velocities for snow grains in still air are between 0.1 and 0.9 m s^{-1} and assume $w_{s0} = 0.5$ m s^{-1}. We

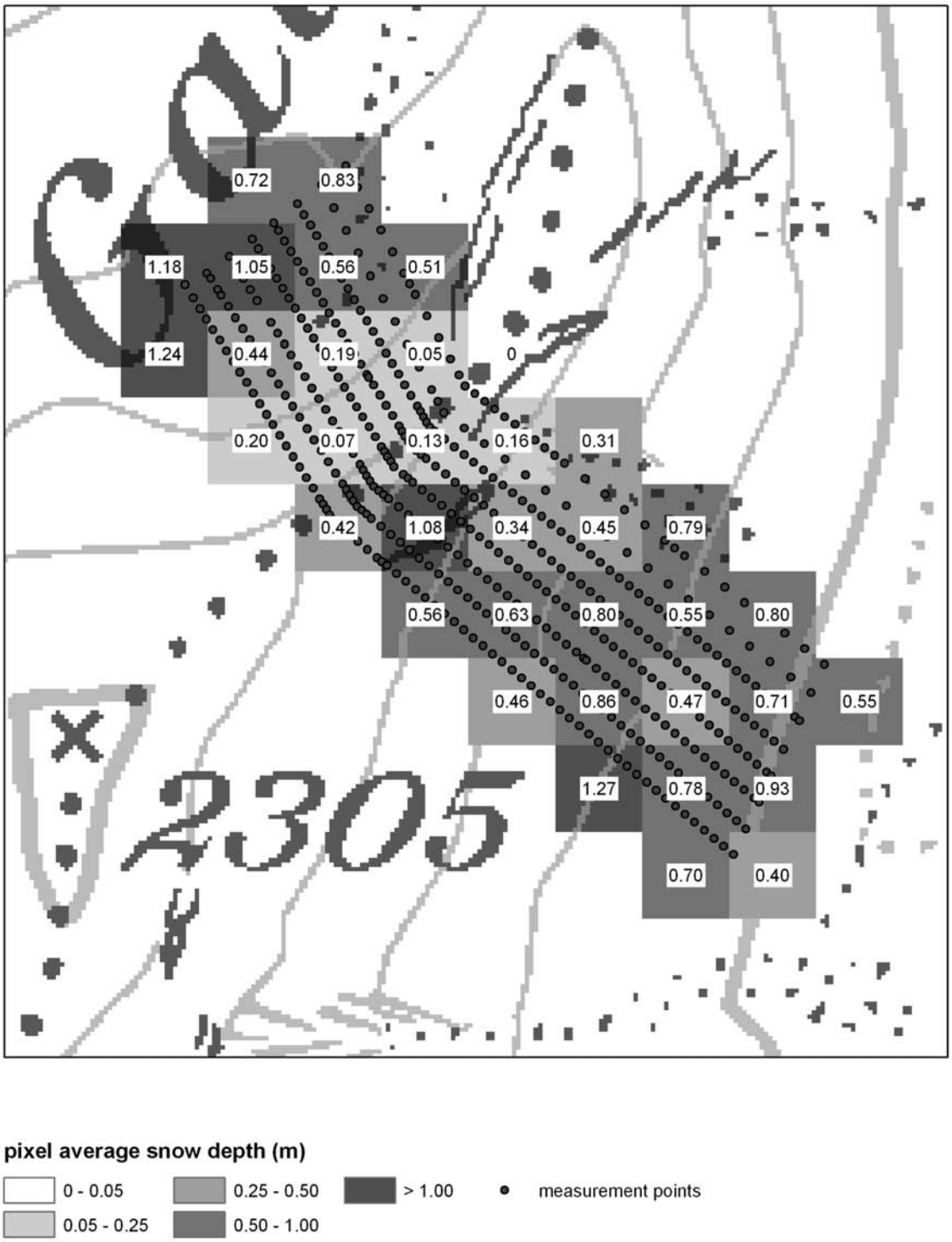

Figure 8. Measured snow distribution for a small stripe over the Gaudergrat ridge. Measurements have been averaged to the pixel resolution of the simulations.

further assume a precipitation rate of 2 mm h^{-1}, which leads to $c_0 = 1.010^{-3}$ kg m^{-3}. On the basis of our measurements of wind speed in the lee and the luff of the Gaudergrat ridge [*Raderschall et al.*, 2008] we can assume friction velocities of 0.25 m s^{-1} and 0.05 m s^{-1} for luff and lee, respectively. According to equation (10), this would translate the settling velocities, w_s, of 0.1 m s^{-1} and 0.45 m s^{-1} for luff and lee respectively. For simplicity, we assume a parcel depth $h = 2$ m and a parcel travel velocity of 3.5 m s^{-1}. Therefore, after a travel distance of only 35 m (10 s), the concentration in the parcel has almost tripled for those numbers and reaches 2.7 10^{-3} kg m^{-3}. Since the deposition is simply the product of local settling velocity and local concentration, we conclude that both processes, the spatially

Figure 9. Digital photograph taken from northern part of Gaudergrat ridge (lee side) on 6 October 2003 after a first snow storm. Areas of average low and high snow can be distinguished.

varying deposition velocities and the associated storage or increased depletion of snow in the air need to considered, since they both have a similar magnitude.

4. Results and Discussion

[33] Below we present an analysis of snow drift over the Gaudergrat ridge from the first major drift event of the extraordinary avalanche period of January and February 1999 and compare the model results to manual measurements. The simulated period starts on 26 January and ends on 31 January. For this period, the snow height development has also been measured. Measurements have been made by manually probing the snow depth along transect lines running across the ridge. The spatial resolution of the measurements is between 2 and 15 m and therefore higher than the current model resolution of 25 m. Before the storm, the snow depth has been measured at about 500 locations to both sides of the ridge. The measurement points have been marked with bamboo sticks. After the storm, the change in snow depth has been measured at exactly the same locations. The period has subperiods between strong to weak winds and zero to heavy precipitation (cf. Figures 1 and 2). In addition to the snow depth, meteorological parameters have been measured at 5 masts equipped with three-dimensional wind probes and standard meteorological sensors [*Raderschall et al.*, 2008].

4.1. Reference Run and Sensitivity to Model Parameters

[34] The model of snow deposition described here tries to implement physical process representation to high degree. However, the complex physics of drifting snow and the range of scales involved still require also significant simplifications. Especially the local processes of erosion, saltation and transition to suspension suffer from the insufficient spatial resolution of the numerical grid close to the surface. In addition, we currently work with one snow grain size only.

[35] One important difference between the conceptual study of preferential deposition discussed above and the numerical simulations is that the effect of turbulence is only represented through the diffusion term in equation (3) and no explicit reduction of the settling velocity as a function of the mean wind speed or the friction velocity is made. This is because of the limitations of equation (10) discussed above.

[36] The effect of many of the simplifications can be assessed by sensitivity studies. For the reference run, we choose to use a fixed settling velocity of 0.5 m s^{-1} and set the parameter controlling the relative height of the saltation mass balance layer to 0.02. The snow distribution after the event is shown in Figure 3 for the full simulation domain and in Figure 4 for the subdomain containing the measurements. Shown are the simulation results, which were initialized with no previous snow and therefore correspond to the snow depth difference measurements. Note that all

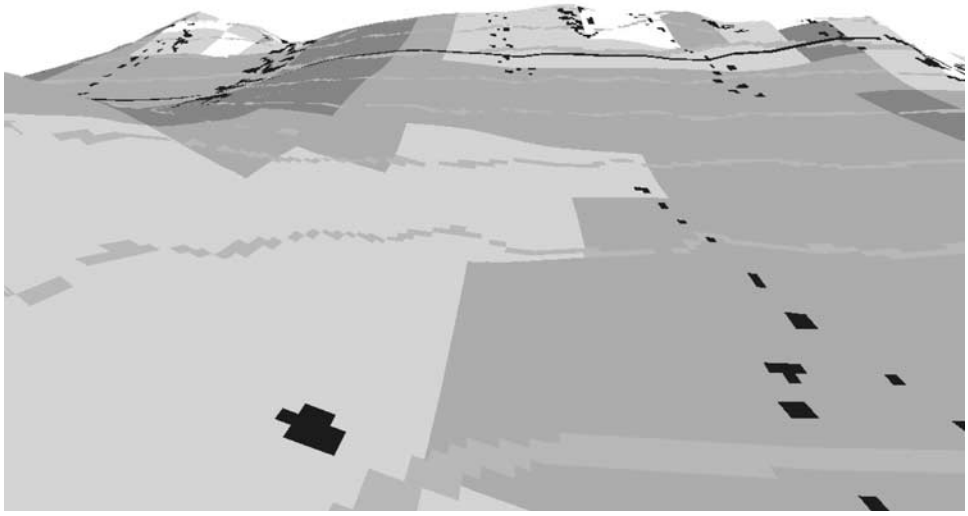

Figure 10. Simulated snow distribution after the first part of the 120 h drift period of January 1999, which may have been comparable to the first snow storm in October 2003. The picture tries to mimic the viewpoint of the photograph in Figure 9.

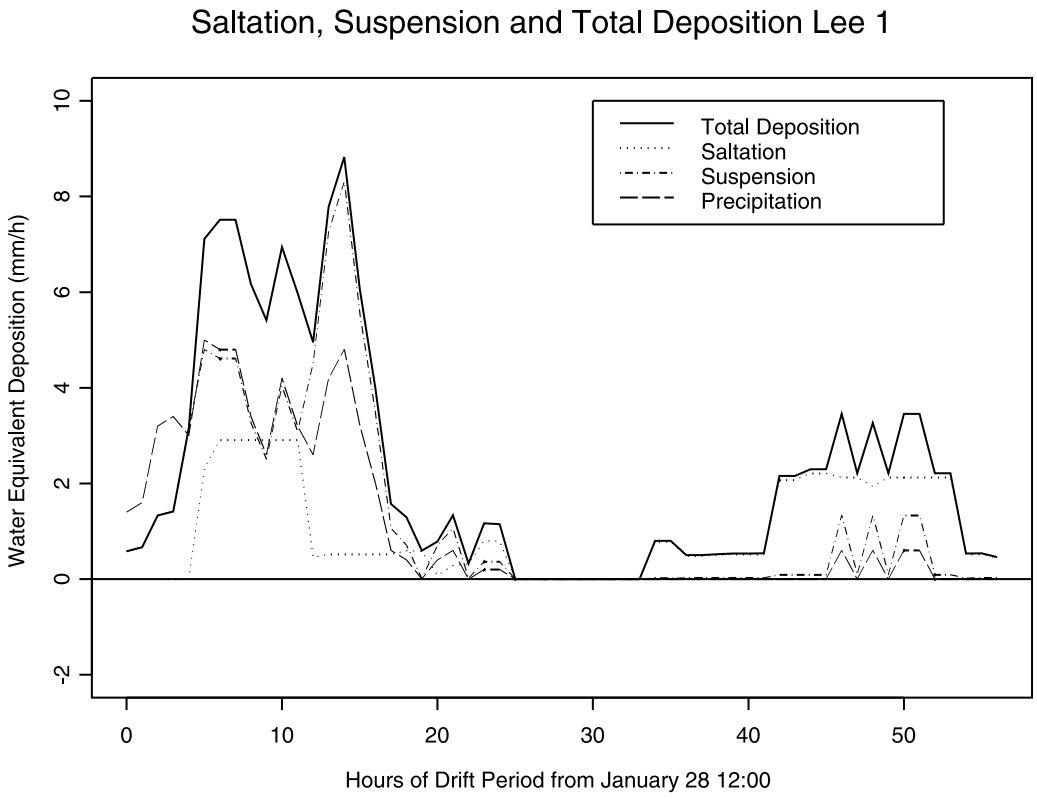

Figure 11. Time series of mean precipitation, total deposition, saltation, and suspension, including preferential deposition for a model pixel in the lee with strong accumulation.

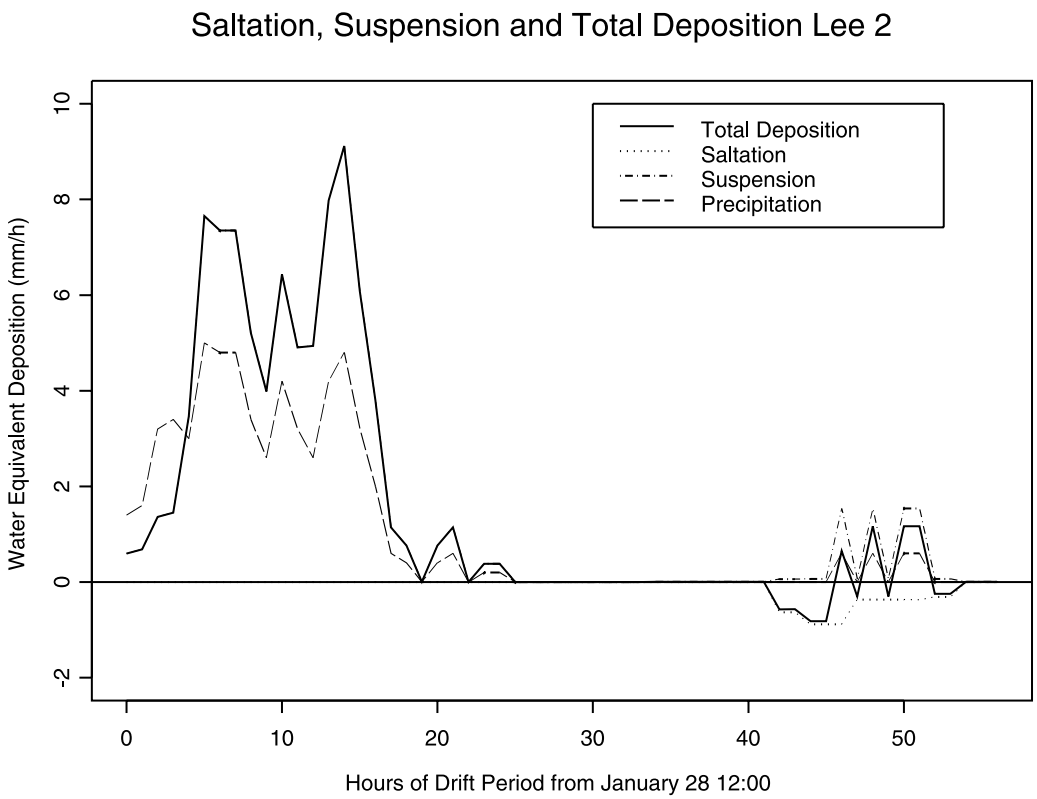

Figure 12. Time series of mean precipitation, total deposition, saltation, and suspension, including preferential deposition for a typical model pixel in the lee at some distance from the ridge.

snow depths presentations are snow depths differences for the drift period discussed. The snow distribution clearly shows distinct areas of erosion and deposition.

[37] As a first sensitivity analysis, we augment the constant settling velocity of the snow grains to 1 m s^{-1}. The corresponding results for the Gaudergrat subdomain are shown in Figure 5. The general pattern of snow distribution is preserved with some local differences. Arbitrarily reducing the threshold friction velocity predicted from SNOWPACK by a factor 0.5 also showed a significant yet not drastic effect. The corresponding results in Figure 6 show more erosion on the windward side of the mountain. As expected, the snow distribution is smoother for a higher settling velocity and more redistribution results from the reduced threshold friction velocity. Altogether, however, the influence of these large parameter changes remain rather small and the general distribution pattern is not changed.

[38] As a further sensitivity, the parameter determining the height of the saltation mass balance was varied from 0.02 (reference run) to 0.2. The model showed almost no sensitivity to this parameter. We finally investigated the sensitivity to the turbulent exchange coefficient in equation (4) and the concentration used as lower BC for the suspension model in equation (2). Multiplying the exchange coefficient by a factor 5 and 0.2, or doubling the saltation concentration, only minor changes in the predicted snow distribution were observed.

[39] The limited influence of the model parameters on the final snow distribution suggests that the snow deposition is mainly determined by convergent and divergent mean flow patterns and the associated vertical velocities.

4.2. Snow Distribution Measured and Simulated

[40] Figure 7 is a full-resolution kriging plot of the measured snow distribution. Comparing to the modelled snow distribution discussed above, it becomes immediately clear that the current model resolution of 25 m is insufficient to capture the small scale variability represented in the measurements in the lee of this very steep slope. Therefore, we restrict ourselves to explore what is possible with the current model resolution of 25 m. The model snow distribution in Figure 4, showing the same area, shows a rather uniform snow distribution with clearly separate erosion (in the luff) and deposition areas.

[41] A better comparison to the measurements is possible, when the measurements are averaged over the pixel size of the model grid. In Figure 8, the averaged measurements are presented. The comparison shows that after the averaging procedure, the measured snow distribution has still a higher variability than the modelled snow distribution. Some features appear to be captured by the model, e.g., that the maximum snow depth is immediately in the lee of the ridge on the southern edge of the measurement area (although not exactly at the same pixel), while to the north, much less snow gets deposited at the same distance to the ridge. The most prominent discrepancy between model and measurement is the missing snow dune (Figure 7) in the luff slope, which forms in a small local depression before the steep part of the luff slope begins. This depression is not present in the 25 m DEM and therefore the associated snow drift cannot be predicted. Overall, the measurements indicate that small terrain features on the scale of meters cause local deposition or erosion, which is superimposed by the larger scale feature

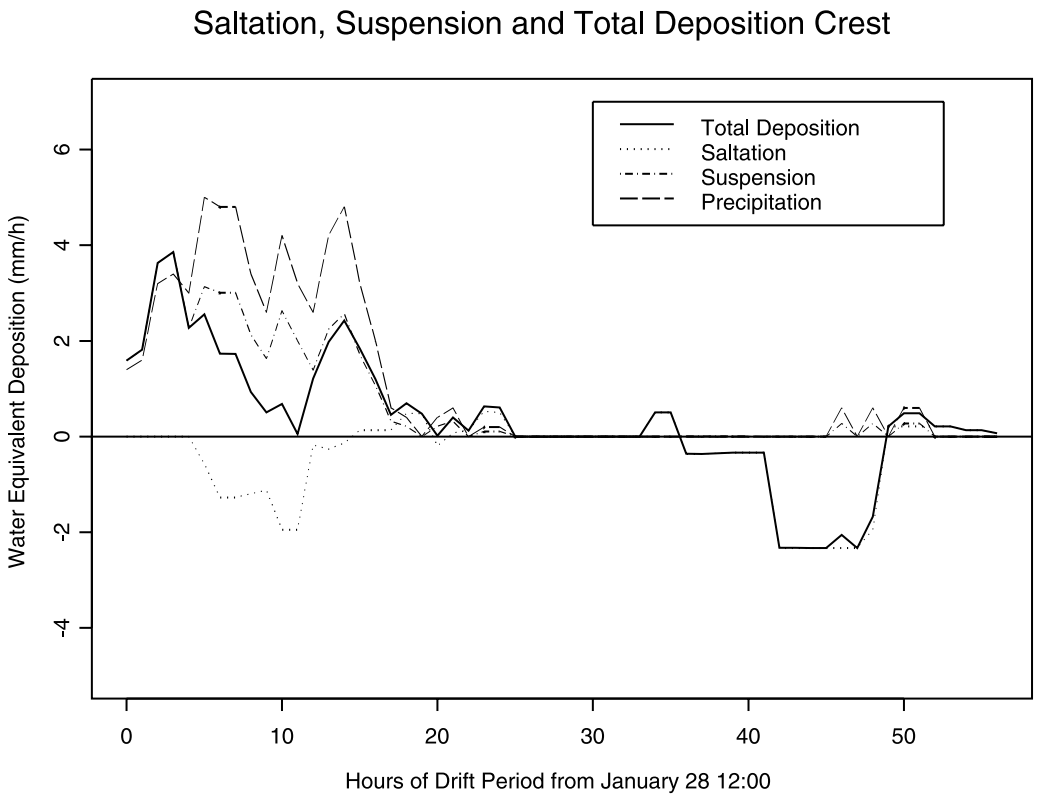

Figure 13. Time series of mean precipitation, total deposition, saltation, and suspension, including preferential deposition for a model pixel at the crest.

that snow gets deposited in the lee of the ridge and not on wind-exposed slopes. The 25 m resolution used for the current simulations appears to capture primarily this larger scale effect.

4.3. Total Snow Transported Over the Ridge

[42] *Doorschot et al.* [2001] developed a simple model of snow transport over mountain ridges by combining an earlier version of the saltation model used here [*Doorschot et al.*, 2004], with a one-dimensional model of suspension and an analytical description of the speed-up over the ridge. This simple model predicts total mass flux (kg m^{-1} s^{-1}) over the ridge at one point and assumes a certain length in the lee slope, over which this mass is distributed. The model showed a very remarkable performance, when Gaudergrat measurements of four drift periods from 2 years were compared to the model predictions. For the data set also analyzed here, model and measurements both show a new snow depth between 0.6 to 0.7 m over the measured area in the lee slope. This is confirmed by our averaged observed distribution in Figure 8. An approximate estimate of the average new snow depth predicted by Alpine3D for the same situation in Figure 4, gives a very similar value of average snow deposition in the lee slope, ranging between 0.5 and 0.8 m at some distance from the ridge.

4.4. Larger-Scale Deposition Patterns

[43] On average, snow drifts always develop at the same locations in the landscape with similar forms over the course of a winter season. This is the reason, why simple snow redistribution codes such as those of, e.g., *Winstral and Marks* [2002] have shown reasonable success in predicting snow distribution. We have tried to show above that the physical model of drifting snow presented here should reflect snow distribution patterns at the ridge scale at the current resolution of 25 m. While we have only a small stripe of measurements from the storm period in 1999, we can roughly infer areas of preferred and reduced snow deposition from a different part of the Gaudergrat ridge by examining a photograph in Figure 9 taken on 6 October 2003 after the first heavy snow storm of that year. On the photograph, areas of enhanced and reduced snow deposition can be distinguished. Figure 10 shows the simulated snow distribution for the 1999 storm period. Figure 10 is a projection of the model result on the topography trying to copy the view of the camera. While contours and distances are not completely unambiguous, it appears that similar areas of preferred snow deposition exist in the photo and the simulation. Note that a small snow slide (avalanche) has occurred in an snow accumulation zone below the ridge left to the erosion area. The erosion area is visible in both, the photo and the simulation. Overall, the comparison can be taken as a rough indication that the model appears to represent the important features of enhanced and reduced deposition at the ridge scale given the fact that we compare patterns from two different storm events of different duration.

4.5. Relative Contribution of Preferential Deposition, Saltation, and Suspension

[44] Having discussed the model behavior in terms of total mass transport and snow distribution, we now want to know, how much the individual processes contribute to snow transport. To this end, we analyze the time series of precipitation, total deposition and the contributions from the

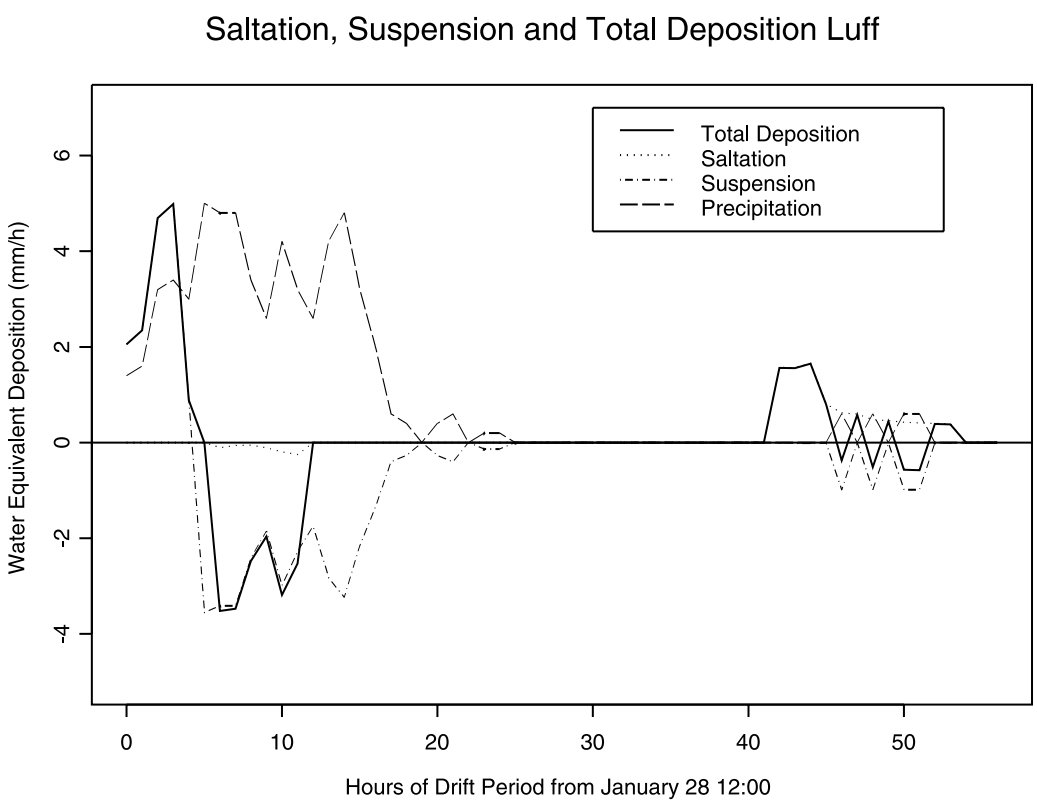

Figure 14. Time series of mean precipitation, total deposition, saltation, and suspension, including preferential deposition for a typical model pixel in the luff at some distance from the crest.

individual transport processes. The second half of the storm period, starting from noon at 28 January, is chosen to illustrate model behavior at selected representative grid points at the windward side (luff), the crest and the lee. Starting with the pixel in the center of the subdomain (cf. Figure 4), which has the highest accumulated snow depth (1.32 m) in the reference run, we illustrate the main features of lee deposition in Figure 11. Initially, during the first 2 h of the period, the pixel receives in the absence of saltation less snow then the mean precipitation over the area. Note that the precipitation curve gives the domain averaged precipitation as measured at an automatic IMIS weather station in a flat field. This precipitation is used as upper and lateral BC for the snow drift simulation. This initial luff pattern quickly changes after hour three, when extra loading of the pixel due to a high saltation flux is visible. After hour 12, the situation changes again and with a continuing small contribution from saltation, the main cause for the high total snow deposition becomes suspension. Overall during this first phase, the deposition is about twice as high as the average over the full domain (precipitation). Then there is a pause in snow deposition around hour 30. During a second phase, which is initially without any precipitation, further loading of the pixel occurs mainly because of saltation alone.

[45] The behavior of a typical pixel in the lee further away from the ridge is illustrated in Figure 12. This pixel has a snow depth of 0.76 m in the reference run and is at a distance of 50 m to the east of the pixel discussed above. In the first and dominant drift phase, this pixel also has greatly enhanced snow deposition when compared to the average precipitation but exclusively due to suspension. Saltation is zero and preferential deposition is the dominant mechanism. In the second phase, not much is happening any more but total deposition is still augmented over precipitation because of suspension, although we here now have a negative contribution of a small saltation flux.

[46] Figure 13 shows the situation of a model pixel at the crest. Presented is the pixel northwest of the first lee pixel discussed above. The pixel has a final snow depth of 0.11 m in the reference run. Deposition of snow due to suspension dominates the first phase, while erosion of the snow cover due to large negative saltation fluxes occurs in the second phase. Note that the pixels in the vicinity of the crest tend to be flat in the digital elevation model in contrast to the sharp crest present in reality.

[47] Finally, we present the situation at the windward side at some distance from the crest. Figure 14 shows the deposition and erosion pattern of the most northwestern pixel within the measurement area. This pixel has a final snow depth of 0.12 m in the reference run. The time series representation of the processes shows that the first phase starts with enhanced accumulation due to preferential deposition at the pixel. This is in agreement with the first phase in the nominal "lee" pixel, which has decreased total accumulation during this time. Then with a change in wind direction, the total accumulation becomes smaller than the average precipitation before significant erosion starts. Toward the end of the first phase, no more accumulation occurs, while the precipitation continues. This is again the counterpart of the increased accumulation in the lee. The second phase is again less important and shows a small accumulation mainly due to saltation.

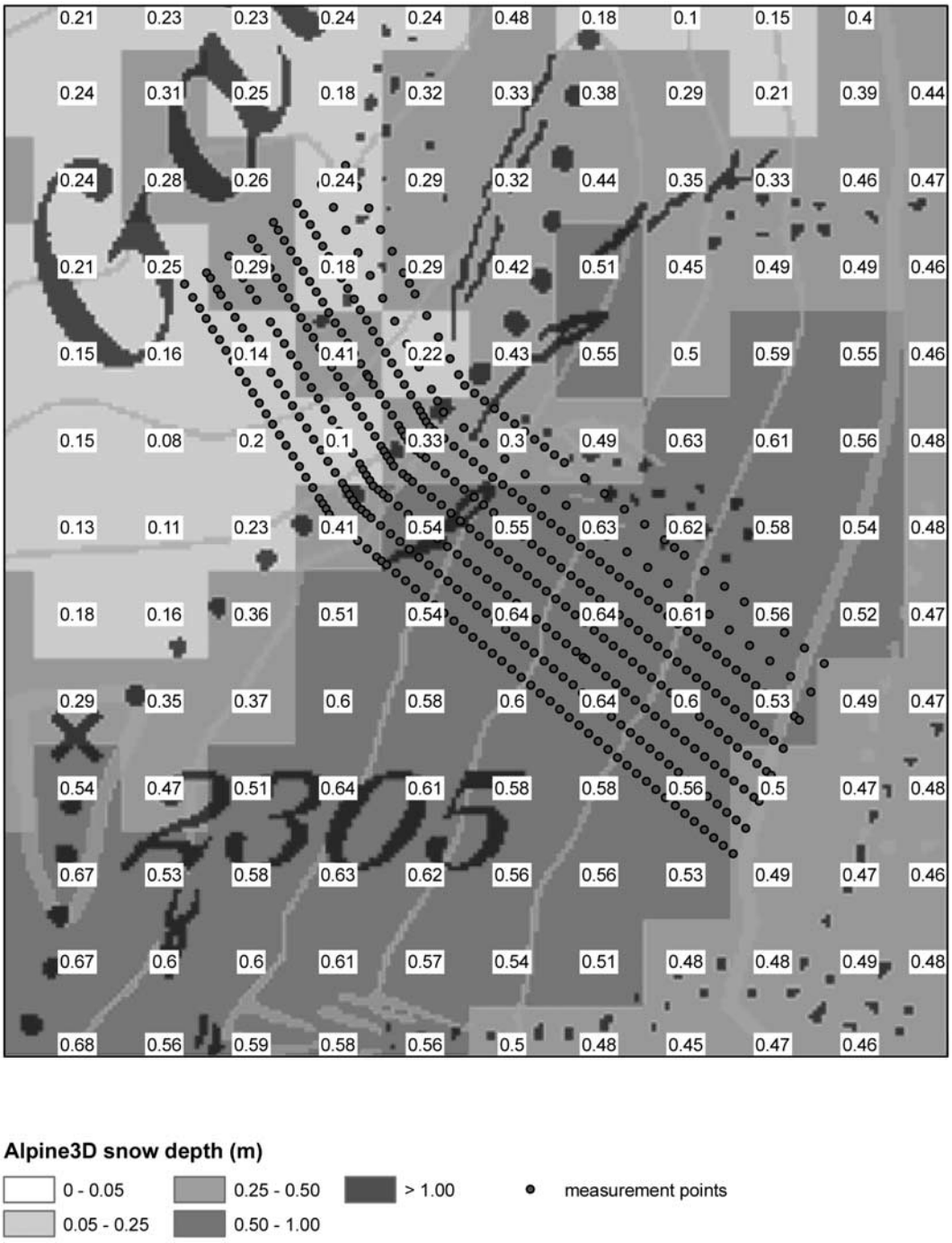

Figure 15. Simulated snow distribution for the Gaudergrat subdomain and the hypothetical case of no saltation.

[48] Since we defined preferential deposition as the interaction between precipitation, flow field and terrain without the influence of erosion and saltation, it is also illustrative to calculate a hypothetical snow distribution when no erosion or saltation is allowed in the model. This snow distribution is presented for the full storm period in Figure 15. Comparing this to the reference run from Figure 4, it becomes clear that saltation is mainly responsible for smaller scale snow redistribution. The general pattern of increased snow deposition in lee slopes is very similar to the "full" simulation, confirming the importance of preferential deposition.

5. Conclusions and Outlook

[49] We have introduced the process of preferential deposition, which is preferred deposition in lee slopes during snow fall in the absence of erosion of already deposited snow and thus also in the absence of saltation. In this context, we discussed the importance of individual processes involved in snow transport and nonuniform snow distri-

bution in steep terrain. To this end, a modeling system that combines high-resolution wind field simulation with snow drift analysis and distributed snow cover simulation has been constructed and presented. The model is complete in the sense that all important processes of topography-snow-drift-atmosphere interactions are represented. The model will be a valuable tool in coming years in the disciplines of hydrology (distribution of snow water content), ecology and biology (snow-wind-vegetation-soil interactions), meteorology (momentum, energy and mass exchanges) and avalanche science. The first results as presented here are encouraging, although the resolution of 25 m employed here, was still insufficient to represent the small scale variability present in the measurements. A main conclusion from the model is that preferential deposition is very significant for the ridge scale snow distribution but that saltation appears to dominate the smaller scale snow deposition patterns. The ridge scale snow distribution is dominated by the angle between the mean wind vector and the topography surface. Other model parameters such as turbulence exchange coefficient or saltation concentration have a very small influence on the final snow distribution. The largest model sensitivity was observed for the mean particle settling velocity and the drift threshold.

[50] Simplifications and limitations of the model presented here are that currently the model is driven by stationary wind fields, which are assumed to represent the situation for 1 h. Consequently, drift is assumed to be stationary, too. This can be an invalid assumption given the very intermittent and nonlinear character of alpine snow drift and has to be further investigated. More fundamentally, the question needs to be explored in how far the highly nonlinear particle transport can be described by only relying on the average flow features as currently done in Alpine3D. Further limitations such as the inadequate horizontal and vertical spatial resolution, the difficulty of formulating a consistent lower boundary condition for drifting snow and the neglect of sublimation and of grain size distributions have been discussed.

[51] Development steps are therefore directed toward a higher horizontal resolution, a two-way coupling between atmospheric model and drift model and a consolidation of the suspension and saltation models. Recently, we were able to measure remotely (laser scanner from airplane) the snow depth change during a drift period for a much larger area than up to now. We expect a major step forward with respect to our model validation efforts from these measurements. We also plan to measure directly concentration distributions on both sides of a similar alpine ridge with new types of lidar and polarimetric radar devices.

[52] This integrated model, which is the first to contain all major factors contributing to the snow loading of avalanche slopes, may also be considered a major step forward in the development of an operational assessment of snow drift for the purpose of avalanche forecasting. It will be used to develop simplified descriptions that can be applied to an even larger area.

[53] Current research work is also dedicated to investigate, how the assumption of a mean flow field can be abandoned and how the full interaction between a turbulent flow and the snow particles can be modelled for our snow drift problems. We also want to understand, how important preferential deposition is for rain precipitation and how it depends on typical terrain features.

[54] **Acknowledgments.** The work is partly funded by the Swiss National Science Foundation and the European Union. Many people contributed to the field campaigns at Gaudergrat. Peter Gauer initiated the measurement setup on the basis of earlier experiences by Roli Meister and Paul Föhn. The Gaudex campaign, during which Figure 9 has been taken, was a collaboration between SLF and Leeds university (Stephen Mobbs). We particularly thank Charles Fierz and Andi Stoffel for help with measurements and GIS and figure making, respectively. Part of the simulations was made using the Advanced Regional Prediction (ARPS) developed by the Center for Analysis and Prediction of Storms (CAPS), University of Oklahoma. CAPS is supported by the National Science Foundation and the Federal Aviation Administration through combined grant ATM92-20009. Two reviewers helped to improve the presentation with many detailed and constructive comments.

References

Bagnold, R. A. (1941), *The Physics of Blown Sand and Desert Dunes*, Methuen, London.

Bartelt, P. B., and M. Lehning (2002), A physical SNOWPACK model for avalanche warning services. part I: Numerical model, *Cold Reg. Sci. Technol.*, *35*(3), 123–145.

Bintanja, R. (2001), Modelling snowdrift sublimation and its effect on moisture budget of the atmospheric boundary layer, *Tellus, Ser. A*, *53*(2), 215–232.

Brooks, A. N., and T. J. R. Hughes (1982), Streamline upwind Petrov-Galerkin formulations for convection dominated flows with particular emphasis on the incompressible Navier-Stokes equations, *Comput. Methods Appl. Mech. Eng.*, *32*, 199–259.

Clifton, A., and M. Lehning (2008), Simulations of wind tunnel snow drift using a semi-stochastic model, *Earth Surf. Processes Landforms*, in press.

Clifton, A., C. Manes, J.-D. Rüedi, M. Guala, and M. Lehning (2007), On shear driven ventilation of snow, *Boundary Layer Meteorol.*, *126*(2), 249–261, doi:10.1007/s10546-007-9235-0.

Déry, S. J., and M. K. Yau (2002), Large-scale mass balance effects of blowing snow and surface sublimation, *J. Geophys. Res.*, *107*(D23), 4679, doi:10.1029/2001JD001251.

Doorschot, J., and M. Lehning (2002), Equilibrium saltation: Mass fluxes, aerodynamic entrainment and dependence on grain properties, *Boundary Layer Meteorol.*, *104*(1), 111–130.

Doorschot, J., N. Raderschall, and M. Lehning (2001), Measurements and one-dimensional model calculations of snow transport over a mountain ridge, *Ann. Glaciol.*, *32*, 153–158.

Doorschot, J., M. Lehning, and A. Vrouwe (2004), Field measurements of snow drift threshold and mass fluxes and related model simulations, *Boundary Layer Meteorol.*, *113*(3), 347–368.

Gauer, P. (2001), Numerical modeling of blowing and drifting snow in alpine terrain, *J. Glaciol.*, *47*, 97–110.

Kind, R. J. (1992), One-dimensional aeolian suspension above beds of loose particles—A new concentration-profile equation, *Atmos. Environ., Part A*, *26*(5), 927–931.

Lehning, M., and C. Fierz (2007), Assessment of snow transport in avalanche terrain, *Cold Reg. Sci. Technol.*, *51*(2–3), 240–252, doi:10.1016/j.coldregions.2007.05.012.

Lehning, M., P. Bartelt, R. L. Brown, T. Russi, U. Stöckli, and M. Zimmerli (1999), Snowpack model calculations for avalanche warning based upon a new network of weather and snow stations, *Cold Reg. Sci. Technol.*, *30*(1–3), 145–157.

Lehning, M., P. B. Bartelt, R. L. Brown, C. Fierz, and P. Satyawali (2002a), A physical SNOWPACK model for the Swiss Avalanche Warning Services. part II: Snow microstructure, *Cold Reg. Sci. Technol.*, *35*(3), 147–167.

Lehning, M., P. B. Bartelt, R. L. Brown, C. Fierz, and P. Satyawali (2002b), A physical SNOWPACK model for the Swiss Avalanche Warning Services. part III: Meteorological boundary conditions, thin layer formation and evaluation, *Cold Reg. Sci. Technol.*, *35*(3), 169–184.

Lehning, M., I. Völksch, D. Gustafsson, T. A. Nguyen, M. Stähli, and M. Zappa (2006), ALPINE3D: A detailed model of mountain surface processes and its application to snow hydrology, *Hydrol. Processes*, *20*, 2111–2128.

Liston, G. E., and M. Sturm (1998), A snow-transport model for complex terrain, *J. Glaciol.*, *44*, 498–516.

Liston, G. E., R. B. Haehnel, M. Sturm, C. A. Hiemstra, S. Berezovskaya, and R. D. Tabler (2007), Simulating complex snow distributions in windy environments using SnowTran-3D, *J. Glaciol.*, *53*, 241–256.

McEwan, I. K. (1993), Bagnold's kink, a physical feature of a wind velocity profile modified by blown sand?, *Earth Surf. Processes Landforms*, *18*, 145–156.

McEwan, I. K., and B. B. Willets (1991), Numerical model of the saltation cloud, *Acta Mech. Suppl.*, *1*, 53–66.

Meister, R. (1987), *Wind Systems and Snow Transport in Alpine Topography*, *IAHS Publ.*, *162*, 265–279.

Nemoto, M., and K. Nishimura (2001), Direct measurement of shear stress during snow saltation, *Boundary Layer Meteorol.*, *100*(1), 149–170.

Nemoto, M., and K. Nishimura (2004), Numerical simulation of snow saltation and suspension in a turbulent boundary layer, *J. Geophys. Res.*, *109*, D18206, doi:10.1029/2004JD004657.

Owen, P. R. (1964), Saltation of uniform grains in air, *J. Fluid Mech.*, *20*, 225–242.

Pomeroy, J. W., and D. M. Gray (1990), Saltation of snow, *Water Resour. Res.*, *26*, 1583–1594.

Pomeroy, J. W., and R. L. H. Essery (1999), Turbulent fluxes during blowing snow: Field tests of model sublimation predictions, *Hydrol. Processes*, *13*, 2963–2975.

Raderschall, N., M. Lehning, and C. Schär (2008), Fine scale modeling of the boundary layer wind field over steep topography, *Water Resour. Res.*, doi:10.1029/2007WR006544, in press.

Sato, T., T. Uematsu, and Y. Kaneda (1997), Application of random walk model to blowing snow, in *Snow Engineering: Recent Advances*, edited by M. Izumi, T. Nakamura, and R. L. Sack, pp. ?–?, Balkema, Rotterdam, Netherlands.

Schmidt, R. A. (1980), Threshold wind-speeds and elastic impact in snow transport, *J. Glaciol.*, *26*, 453–467.

Shao, Y., and A. Li (1999), Numerical modelling of saltation in the atmospheric surface layer, *Boundary Layer Meteorol.*, *91*(2), 199–225.

Stull, R. B. (1988), *An Introduction to Boundary Layer Meteorology*, 1st ed., Kluwer Acad., Dordrecht, Netherlands.

Sundsbø, P. A., and E. W. M. Hansen (1997), Modelling and numerical simulation of snow drift around snow fences, in *Snow Engineering: Recent Advances*, edited by M. Izumi, T. Nakamura, and R. L. Sack, pp. ?–?, Balkema, Rotterdam, Netherlands.

Takeuchi, M. (1980), Vertical profile and horizontal increase of drift-snow transport, *J. Glaciol.*, *26*, 481–492.

Winstral, A., and D. Marks (2002), Simulating wind fields and snow redistribution using terrain-based parameters to model snow accumulation and melt over a semi-arid mountain catchment, *Hydrol. Processes*, *16*, 3585–3603.

Xiao, J., R. Bintanja, S. J. Déry, G. W. Mann, and P. A. Taylor (2000), An intercomparison among four models of blowing snow, *Boundary Layer Meteorology*, *97*(1), 109–135.

Xue, M., K. K. Droegemeier, V. Wong, A. Shapiro, and K. Brewster (1995), ARPS version 4.0 user's guide, 380 pp., Cent. for Anal. and Predict. of Storms, Univ. of Okla., Norman, Okla.

M. Lehning, H. Löwe, N. Raderschall, and M. Ryser, WSL, Swiss Federal Institute for Snow and Avalanche Research, SLF Davos, Flüelastr. 11, CH-7260 Davos Dorf, Switzerland. (lehning@slf.ch)